Nonlinear dynamics control of GaAs nanomechanical resonator using laser

To cite this article before publication: Leisheng Jin *et al* 2021 *Nanotechnology* in press https://doi.org/10.1088/1361-6528/abf3f1

Nonlinear dynamics control of GaAs nanomechanical resonator using laser

Leisheng Jin*[1], Hao Zhao[1], Zhi Li[1], Zongqing Jiang[1], Lijie Li[2], Xiaohong Yan[1]

1. College of Electronic and Optical Engineering and College of Microelectronics, Nanjing University of Posts and Telecommunications, Nanjing 210023, China;
2. College of Engineering, Multidisciplinary Nanotechnology Center, Swansea University, Swansea SA2 8PP, UK

E-mail: jinls@njupt.edu.cn

Nov. 2020

Abstract. To control, manipulate and read-out nanomechanical resonators is of great significance for many applications. In this work, we start by constructing a nonlinear dynamical model that is deduced from the fundamental beam, photon-electron interaction and energy band theories, with the aim to describe a complicated cavity-less optomechanical coupling process. Based on the established model, the manipulation on resonator's response including soften and hardening effect due to laser injection is firstly revealed. Taking the form of the laser parametric driving, the controlling on resonator's dynamics, in particular the nonlinear regime, is comprehensively investigated. It is found that both the laser power and frequency can be used for direct manipulating the NEMS resonator's dynamics, such as amplitude amplification, periodicity changing and periodic-chaotic state conversion. Bifurcation diagrams are given subsequently manifesting a deterministic dynamics evolving route. Finally, the controlling on chaotic states of the nanomechanical resonator using laser parametric driving is specially studied. The Max lyapunov Exponents together with time series calculation show that the chaotic states can be controlled at a few certain frequency points of the injecting laser. The work not only provides the guidance for using laser to control nanoscale resonators, but also sheds light in exploring novel applications based on nonlinear NEMS resonators.

Keywords: Optomechanical coupling, Optical absorption, Chaos, Parametric, Bifurcation

1. Introduction

Nano-Electromechanical System (NEMS) resonators, well known for their extremely high frequencies, high mechanical responsivity and large quality factors[1], are widely used in highly efficient/low-noise transducers[2] and ultra-sensitive sensors[3]. In contrast to their MEMS counterparts, they inherently exhibit rich nonlinear dynamics including chaos and bifurcation[4][5]. Currently, NEMS resonators are deeply

participating in the development of nano-opto-electro-mechanical systems (NOEMS)[6], expanding their applications further to the fields of quantum-limited measurement[7], optomechanical entanglement[8], multi-physics interfaces[9], optofluidics sensors[10], etc. As the electromechanical systems are miniaturized continuously, to control, manipulate and readout of the mechanical motion becomes increasingly changeable. Traditionally, parametric effect utilizing capacitive and piezoelectric means to modulate the spring constant of the NEMS resonator are adopted[11][12]. In cavity-optomechanics, self-feedback originated from the pressure or photothermal backaction onto the mechanical resonator is employed to cool and amplify the mechanical motion[13]. Though highly tunable control of a single nanomechanical resonator can be achieved, there are roadblocks in applying these methods to a broader scope which mainly includes integrated nanomechanical systems such as nanomechanical circuits and sensor arrays[14][15]. Recently, a cavity-less optomechanical coupling scheme is experimentally realized in III-V semiconductor micro-mechanical systems, which sheds light in the development of functional integrated optomechanical devices[16]. In their work, a GaAs-based heterostructure cantilever is fabricated, and by taking the advantage of opto-piezoelectric backaction, the self-feedback cooling and amplification of the thermomechanical motion can be realized through detuning the photon energy from the exciton resonance. However, the study is still restricted in the linear regime, aiming at micro-single-clamped cantilevers. The double-clamped nonmechanical resonators that are characterised by exhibiting complicated nonlinear dynamics, as stated earlier, are beyond the scope of the research. It is known that the nonlinear behaviors produced by NEMS resonators play an important role in device and system operation. To control and/or utilize these behaviours with an efficient way is of great significance for many practical applications[17][18][19][20].

In this work, we start with the dynamical model of a double-clamped NEMS resonator using Euler-Bernoulli beam theory. Then, we, in depth, develop the calculation process of optical absorption rate in a cavity-less optomechanical coupling scenario based on the Fermi-Golden rule, and by determining the relationship between the absorption rate and the tensile stress produced in the beam due to optopiezoelectric effect, a multi-physical dynamical model that incorporates optical, mechanical and electrical mode is for the first time constructed. Based the constructed model, it is revealed that the laser injection can bring softening and hardening effect to the NEMS resonator fabricated with different orientated-GaAs material. Furthermore, the parametric manipulation of the NEMS resonator using laser is investigated. Both the laser power and frequency are found to have a direct impact on affecting the nonlinear dynamics of the resonator, with both the bifurcation phenomenon having chaos and amplitude amplification revealed, which has huge potential in future optical control, readout and manipulation of the NEMS resonators. Finally, we focus on chaos control by using parametric laser driving. A few certain frequencies of pumping laser are proved to be effective in converting chaotic state of NEMS resonator into periodical states. Our work lays foundation for exploring novel optical-NEMS based applications

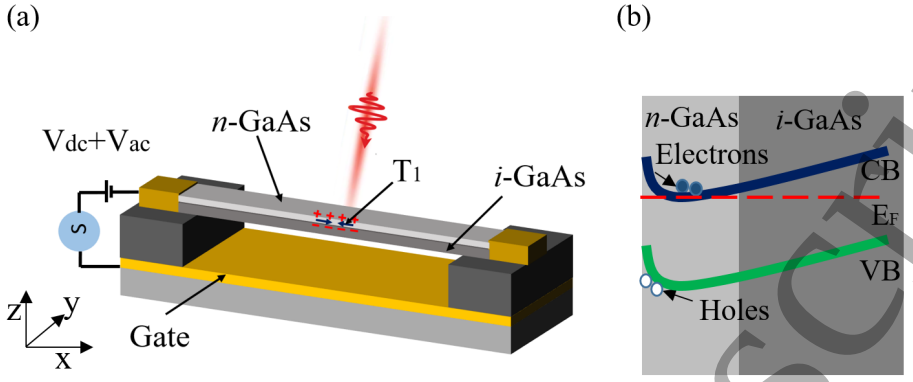

Figure 1. (a) Schematic diagram of the GaAs resonator with laser modulation. (b) Energy band diagram of GaAs resonator with light generated electron-hole pairs appeared to be separated by built-in field.

that, in particular, involves nonlinear dynamics, and also sheds light in developing integrated means for reading out, controlling and manipulating the weak signals of NEMS resonators.

2. Theory and Model

The nanoelectromechanical resonator we study in this work is schematically shown in Fig. 1 (a). It mainly consists a doubly-clamped GaAs beam, of which about one thirds the whole thickness is N-type (Si) doped, and the rest is intrinsic. In such a structure, the Si doping and the pinning of the Fermi level can induce a built-in field in the direction perpendicular to the surface as shown in Fig. 1(b). When there is a laser focused on the beam, many electrons and holes are expected to appear in the N-GaAs layer due to the optical absorption, and these electron-hole pairs are separated by the built-in field. Because of the nonzero piezoelectric constant ($D \neq 0$) in the GaAs materials, the optopiezoelectric effect arises as indicated by the black arrow in Fig. 1 (a). Note that the direction of the piezoelectric effect, represented by the T_1, is reversed between the [110] and [$\bar{1}$10] orientated GaAs beam. The T_1, therefore, is tensile or compressive, which plays an essential role in manipulating and controlling the dynamics of the NEMS resonator as described later. The electromechanical driving force for the resonator is applied through an AC and DC gate voltage, i.e., $V_{dc} + V_{ac}$, where V_{ac} is with frequency ω_d. The dynamical model for the resonator is given by:

$$EI\frac{\partial^4 W}{\partial x^4} + \rho A\frac{\partial^2 W}{\partial t^2} + c\dot{W} - \left[T_0 + T_1 + \frac{EA}{2L}\int_0^L \left(\frac{\partial W}{\partial x}\right)^2 dx\right]\frac{\partial^2 W}{\partial x^2} = F_E \qquad (1)$$

where W is the displacement of the beam in z-direction, E is Youngs modulus, I is the area moment of inertia, ρ is the density, A is the cross-sectional area, L is the length of the resonator beam, F_E is distributed force applied on the beam, which can be expressed as:

$$F_E = -\frac{\pi\varepsilon V^2(t)}{(W(x,t)+d)\left[ln\left(4\frac{W(x,t)+d}{r}\right)\right]^2} \approx -\frac{2\pi\varepsilon V_{dc}V_{ac}cos(\omega_d t)}{h\left(ln\frac{4d}{r}\right)^2} = F_0 cos(\omega_d t) \quad (2)$$

where ε is the dielectric constant of the gaseous medium surrounding the resonator, d is the initial distance between the beam and the gate. For deriving Eq. (2), the approximation is made based on the assumption that the displacement of the beam is much smaller than the gap d. In addition, only the harmonic term $2V_{dc}V_{ac}cos(\omega_d t)$ contributing to the force is kept, with the static and not resonant terms omitted. The omitted terms, together with fabrication imperfections, link to the initial tension in the beam, and correspondingly we incorporate an initial term T_0 into the dynamical model described by Eq. (1). The damping ratio $c = -(\pi P d)/(4v_T)$, where P is the air pressure and $v_T = \sqrt{k_B T_k/m}$ represents the air molecule velocity at temperature T_k, with k_B and m denoting the Boltzmann constant and the molecular mass of air, respectively. In order to conduct a numerical analysis based on Eq. (1), the well-known Galerkin's method[21] can be employed. Specifically, the displacement $W(x,t)$ can be written as: $W(x,t) = z(t)\phi(x)$, where $\phi(x) = (2/3)^{1/2}[1 - cos(2\pi x/L)]$ and $z(t)$ are the deflection eigenmode and displacement at the center point of the beam, respectively. $\phi(x)$ satisfies the boundary condition: $\phi(0) = \phi(L) = \phi''(0) = \phi''(L)$. By substituting $W(x,t) = z(t)\phi(x)$ into Eq. (1), multiplying $\phi(x)$ on both side of Eq. (1) and then integrating the equation from 0 to L, the dynamical equation describing the displacement of the beam can be obtained:

$$\left(\rho AL + \frac{4\pi^2}{3L}\rho I\right)\ddot{z} + cL\dot{z} + \left(EI\frac{16\pi^4}{3L^3} + (T_0+T_1)\frac{4\pi^2}{3L}\right)z + \frac{EA}{2L}\left(\frac{16\pi^4}{9L^2}\right)z^3 = \frac{-2\pi\varepsilon V_{dc}V_{ac}}{h(ln(4h/d))^2}\sqrt{2/3}Lcos(\omega_d t) \quad (3)$$

During the process for deriving Eq. 3, the following integrals are used:

$$\int_0^L (d^2\phi/dx^2)^2 dx = \frac{16\pi^4}{3L^3}; \int_0^L \phi^2 dx = L; \int_0^L (d\phi/dx)^2 dx = \frac{4\pi^2}{3L}; \int_0^L \phi dx = \sqrt{\frac{2}{3}}L \quad (4)$$

Before further conducting the numerical analysis of Eq. (3), one has to also clarify the term T_1. As discussed above, it is closely related to the optical absorption, and thus the optical transitions rate of the GaAs needs to be firstly considered. According to the Fermi's golden rule[22], the optical transitions rate $W_\uparrow(\overrightarrow{k}_i)$, representing the transition rate of an electron from the initial state in valance band to a state in the conduction band in the presence of electromagnetic radiation, is given by:

$$W_\uparrow(\overrightarrow{k}_i) = \frac{2\pi}{\hbar}\left(\frac{qA_0}{2m}\right)^2 |\hat{\overrightarrow{p}}_{cv}\cdot\hat{n}|^2\delta(E_c(\overrightarrow{k}_i) - E_v(\overrightarrow{k}_i) - \hbar\omega) \quad (5)$$

where $\hbar$ is Plank constant divided by 2π, q is the charge of an electron, and A_0 is the amplitude of vector potential $\overrightarrow{A}(\overrightarrow{r},t)$ which is used for defining electric and magnetic field of electromagnetic radiation. The $|\hat{\overrightarrow{p}}_{cv}\cdot\hat{n}|^2$ is squared momentum matrix element, which depends on the electron wavevector $\overrightarrow{k}_i$ and the polarization direction of the electromagnetic wave. In the delta function, $E_c(\overrightarrow{k}_i)$ and $E_v(\overrightarrow{k}_i)$ are energy of an electron with a particular wavenumber $\overrightarrow{k}_i$ in the conduction band and valance band, respectively, and they have a energy gap $\hbar\omega$ corresponding to a photon energy. Based on Eq. (5), it is straightforward to have the transitions happening per unit volume of the material per second, which can be expressed, as:

$$R_{\uparrow}=\frac{2}{V}\times\sum_{\overrightarrow{k}_i}W_{\uparrow}(\overrightarrow{k}_i)f_v(\overrightarrow{k}_i)[(1-f_c\overrightarrow{k}_i)] \tag{6}$$

where the $f_v(\overrightarrow{k}_i)$ and $(1-f_c\overrightarrow{k}_i)$ represent the probability of a electron and hole in valance band and conduction band, with $f_{v(c)}$ denoting Fermi-Dirac probability function. The summation term in Eq. (6) can be written into the integral form covering all the wavenumbers in the first Brillouin zone (FBZ), i.e., $\sum_{\overrightarrow{k}_i}\rightarrow\int_{FBZ}d^3\overrightarrow{k}_i/(2\pi)^3$, and the Eq. (6) can be specifically written as, :

$$\begin{aligned}R_{\uparrow}(\omega)&=\frac{2\pi}{\hbar}\left(\frac{qA_0}{2m}\right)^2\left\langle|\hat{\overrightarrow{p}}_{cv}\cdot\hat{n}|^2\right\rangle\\&\times2\int_{FBZ}\frac{d^3\overrightarrow{k}_i}{(2\pi)^3}f_v(\overrightarrow{k}_i)[(1-f_c\overrightarrow{k}_i)\delta(E_c(\overrightarrow{k}_i)-E_v(\overrightarrow{k}_i)-\hbar\omega)\end{aligned} \tag{7}$$

, in which $|\hat{\overrightarrow{p}}_{cv}\cdot\hat{n}|^2$ has been replaced by its average value, and can be pulled out from the integral. In most bulk III-V semiconductors with cubic symmetry the average value$\left\langle|\hat{\overrightarrow{p}}_{cv}\cdot\hat{n}|^2\right\rangle$ does not depend on the polarization direction of the electromagnetic wave. In Eq. (7), m_r is the reduced mass and defined by: $1/m_r=1/m_e+1/m_h$, where m_e and m_h are effective mass of an electron and hole, respectively. Likewise, the stimulated emission in the GaAs can also be obtained, as:

$$\begin{aligned}R_{\downarrow}(\omega)&=\frac{2\pi}{\hbar}\left(\frac{qA_0}{2m}\right)^2\left\langle|\hat{\overrightarrow{p}}_{cv}\cdot\hat{n}|^2\right\rangle\\&\times2\int_{FBZ}\frac{d^3\overrightarrow{k}_i}{(2\pi)^3}f_c(\overrightarrow{k}_i)[(1-f_v\overrightarrow{k}_i)\delta(E_c(\overrightarrow{k}_i)-E_v(\overrightarrow{k}_i)-\hbar\omega)\end{aligned} \tag{8}$$

If we consider a semiconductor in which the conduction band and valence band energy dispersions are given by $E_c(\overrightarrow{k})=E_c+\hbar^2k^2/(2m_e)$ and $E_v(\overrightarrow{k})=E_v-\hbar^2k^2/(2m_h)$, the net photon absorption rate is obtained as:

$$\begin{aligned}\alpha(\omega)&=\frac{R_{\uparrow}(\omega)-R_{\downarrow}(\omega)}{n_p\frac{c}{n_g^M}}\\&=\left(\frac{q}{m}\right)^2\left(\frac{\pi}{\varepsilon n\omega c}\right)\left\langle|\hat{\overrightarrow{p}}_{cv}\cdot\hat{n}|^2\right\rangle\frac{1}{2\pi^2}\left(\frac{2m_r}{\hbar^2}\right)^{3/2}\sqrt{\hbar\omega-E_g}\\&\times\left[f_v\left(E_v-(\hbar\omega-E_g)\frac{m_r}{m_h}\right)-f_c\left(E_c+(\hbar\omega-E_g)\frac{m_r}{m_e}\right)\right]\end{aligned} \tag{9}$$

where c/n_g^M is the velocity of the photons with c and n_g^M representing the velocity of light and the refractive index of GaAs, respectively, n_p is number of photons per unit volume, i.e., photon density, which is related with vector potential by $n_p = (1/2)(\omega^2/\hbar\omega)nn_g^M\varepsilon_0|\overrightarrow{A}_0|^2$.

With having the net absorption rate, the rate of carrier generation in the N-GaAs layer is given by:

$$G_{eh} = \frac{P_{ex}\lambda_{ex}}{c_1}(1 - e^{-\alpha(\omega)t_1}) \tag{10}$$

where P_{ex} and λ_{ex} are power and wavelength of injecting laser, respectively. c_1 is constant and t_1 is the thickness of N-CaAs layer. The number of generated electron-hole pairs are decided by the rate equation:

$$\frac{dn}{dt} = G_{eh} - \frac{n_{eh}}{\tau} \tag{11}$$

where τ is the nonradiative recombination lifetime. Last, the indced optopiezoelectric force $T_1 = n_{eh}D$, where D is the piezoelectric constant. Note that in the above analysis we mainly adopt the classical approach to deal with it, i.e., opto-electromechanical coupling. The phonon interaction does exist. During the vibration of beam, the strain can modulate the band structure to some extent, the so-called deformation potentials, due to which the band gap would change somehow and further affect the absorption rate. However, in our following simulations, the strain induced by the vibration is relatively small, under which the deformation potential generated could not bring an obvious change to the band gap and its related absorption rate as well as generated electron-hole pairs. In addition, the sample heating by laser irradiation is experimentally found to be negligible[23], and it is not considered in this study.

3. Numerical Analysis

Combining Eqs. (3-11), the interplay between injecting laser and the dynamics of the resonator is investigated in this section. During the following simulations, $T = \omega_0 t$ and $Z = z/d$ are used throughout for normalizing. First, the bandstructure of GaAs taking spin-orbit interaction into account are calculated by using $k \cdot p$ theory[24]. The result is shown in Fig. 2 (a), where the Γ-X direction is plotted along the positive axis while the Γ-L direction is plotted along the negative axis. The energy gap E_g at the Γ point between valance and conduction band decides the optical absorption. The result of laser-induced tension, T_1, calculated using Eqs. (9-11), is presented in Fig. 2 (b), in which how the values of tension T_1 changes with light power P_{ex} and wavelength λ_{ex}, varying in [1 100]nW and [690 1200]nm, respectively, are given. One can see that the T_1 is increased with light power linearly but peaked at about $\lambda = 840nm$ corresponding to the absorption edge of N-GaAs. Other parameters used are summarized in Table 1, and they are kept constant in the following simulations unless specifically indicated.

Table 1. Parameters taken for numerical analysis.

Mechanical	Values	Optical	Values
L/W	$3{\times}10^3/150$ nm	r_0	2 nm
t_1/t_2	20/40 nm	$\hbar$	$6.626 \times 10^{-34}\ J \cdot s$
E	85.5×10^9 Pa	D	-1.35×10^{-12} C/N
d	200 nm	τ	1.6×10^{-7} s
ρ	5332 kg/m^3	E_g	1.424 eV
m_0	5.6×10^{-24} kg	m_e/m_h	$0.067/0.45 \cdot 9.11 \times 10^{-32}$ kg
T_0	3×10^{-9} nN	n_g^M	3.9476

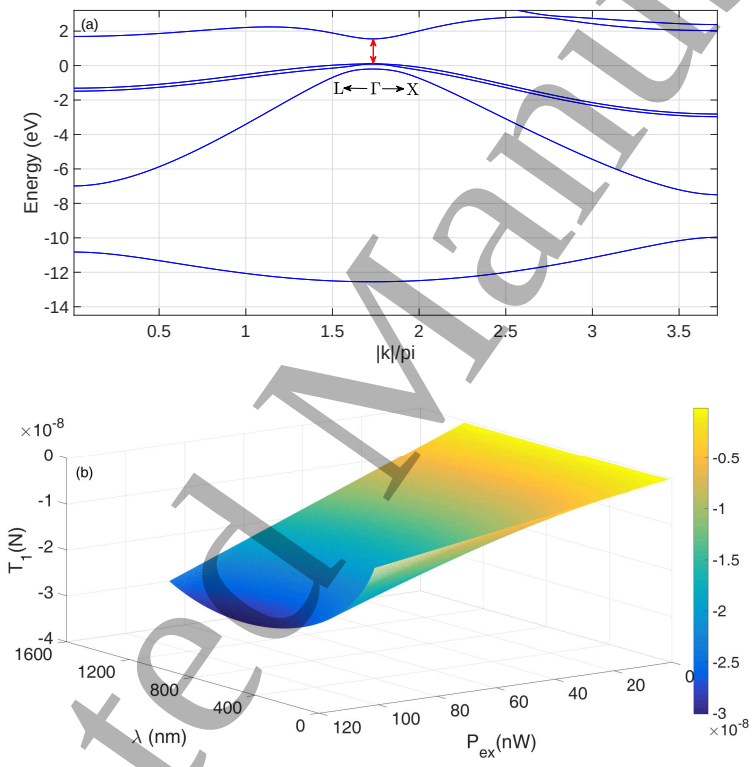

Figure 2. (a) Bandstructure of GaAs taking spin-orbit interaction into account calculated by using k·p theory, in which the red arrow indicates the energy gap corresponding to the optical absorption. (b) Laser-induced tension T_1 calculated with varying laser power and wavelength.

3.1. Softening and Hardening Effect

When the applied voltage is relatively low, e.g., $V_{dc} = V_{ac} = 5$ V, that the resonator oscillates in periodical state, the impacts on intrinsic dynamics made by the focused laser are studied. Typical results reflecting the softening and hardening effect due to laser are given. It is shown in Fig. 3 that in [110] and [$\bar{1}$10] orientated GaAs beam, respectively, the intrinsic dynamics can be further tuned into hardening resonance and softening response using low-powered laser ($\approx 2.48\mu W$). In fact, a wide tunability of the resonant frequency can be achieved, though only partial results are present here.

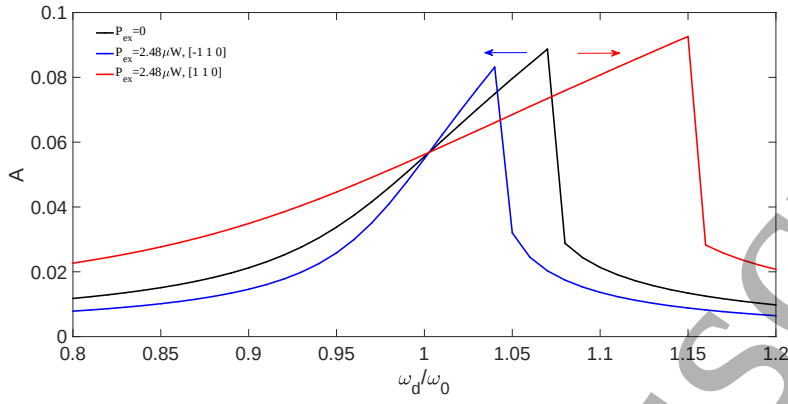

Figure 3. Softening and hardening effect in GaAs resonator brought by laser irradiation. The red and blue curve corresponding to [110] and [$\bar{1}$10] orientated beam.

3.2. Parametric Driving Effect

Parametric driving is widely used in signal processing with nanoscale devices. Here, we study how an external laser can be employed for modulating the dynamics of CaAs NEMS resonator. In this study, the power of the injecting laser is applied in the form: $P_{ex} = P_{ex0}sin(w_p t)$, with the amplitude P_{ex0} fixed at 1.24 μW and the frequency w_p varied in [1 5]ω_0, where the ω_0 is the natural frequency of the resonator. The laser beam is focused on the center of the resonator beam. The driving voltage V_{dc} and V_{ac} are all set to be 5 V. The driving frequency ω_d is swept in the range of [0.8 1.2]ω_0. Other parameters are adopted according to Table. 1. First, the amplitudes of the resonator are calculated under different parametric driving frequency as shown in Fig. 4 (a-c). It is found that the amplitude of resonator exhibits complicated performance. Specifically, in Fig. 4 (a), when $w_p \in$[1 1.6]ω_0, the amplitudes are not smoothly increased but with ups and downs, different from the case without parametric driving when the driving frequency ω_d is located in the range of [0.8 1.05]ω_0. This is attributed to the modulating effect brought by parameter driving. However, when the parametric driving frequency is relatively larger than ω_0, i.e., $w_p \in$[4 4.6]ω_0, there seems no modulating effect existing anymore. The result is shown in Fig. 4 (c). It can be concluded that only when the parametric driving is applied during the intrinsic period of GaAs resonator, the laser parametric driving can exsert an obvious effect. Now, let us study the case when $w_p \in$[2 2.6]ω_0 as shown in Fig. 4 (b), where it is shown that the amplitudes of GaAs resonator are amplified. This is, to some extent, consisted with result that periodic modulation of the spring constant of the system at twice its fundamental resonance frequency can have an apparent amplitude increase[25]. To further illustrate the modulating and amplifying effect made by laser parameter driving, the bifurcation diagram of amplitude versus w_p is given in Fig. 5. It is clearly shown that there are three regions can be categorized. The first is located when $w_p \in$ [1.5 1.9], in which the parametric driving fluctuates the intrinsic response. The second lies in $w_p \in$ [2 2.3]ω_0, in which the amplitude is mostly amplified. In the third region, the amplitude of the GaAs is without obvious changes.

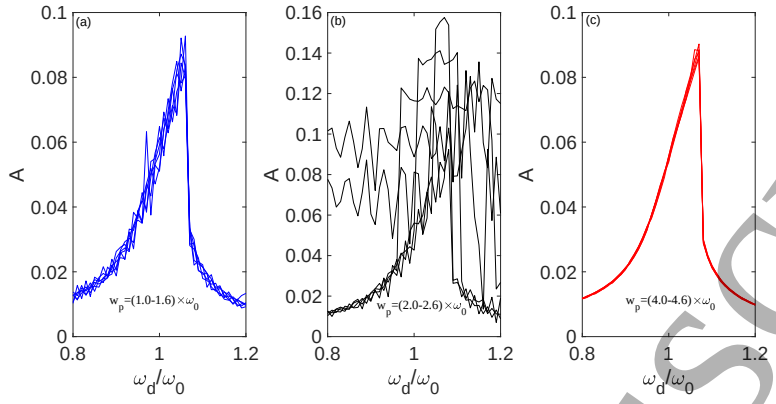

Figure 4. Resonances performance in terms of amplitude of GaAs driven by parametrical laser at different frequency. (a) $w_p \in[1\ 1.6]\omega_0$; (b) $w_p \in[2\ 2.6]\omega_0$; (c) $w_p \in[4\ 4.6]\omega_0$.

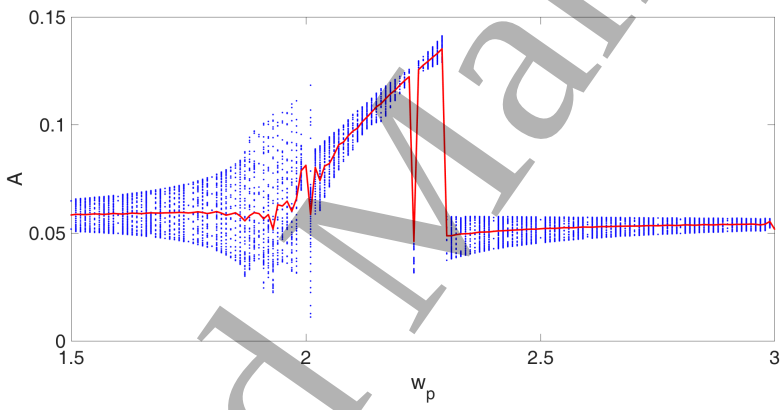

Figure 5. Amplitudes bifurcation diagram with parametric driving frequency w_p varied in the range of $[1.5\ 3]\omega_0$ and the amplitude P_{ex0} fixed at 1.24 μW.

The red solid line in Fig. 5 indicates the mean values of the amplitudes. There is one drop point in the region 2. The reason for this is that in the region the resonator vibrational amplitude can be amplified to some extent. The amplification or so-called the gain is actually the nonlinear function of external driving phase ϕ, external driving strength F_0 and parametric driving frequency w_p, and particularly sensitive with the ϕ. For $\phi = 0$, the gain could reach minimum at some point as w_p varying[26]. Note that during the calculation of results in Fig. 5, the electromechanical driving is fixed, i.e., $V_{dc} = V_{ac} = 5$ V and ω_d=ω_0. In addition, typical results of time series of the GaAs resonator are further given in Fig. 6, proving the modulating effect reflected in above analysis. In Fig. 6 (a-d), the time series versus time T when $w_p = 1.52\omega_0$, $w_p = 1.88\omega_0$, $w_p = 2.27\omega_0$, and $w_p = 3\omega_0$ are plotted, and these results manifests the modulating and amplifying effect brought by laser in Fig. 4 and 5, respectively.

In Fig. 7, we further characterize the modulation effect of parametric driving by fixing the parametric driving frequency $w_p = 2.12\omega_0$. The parametric driving

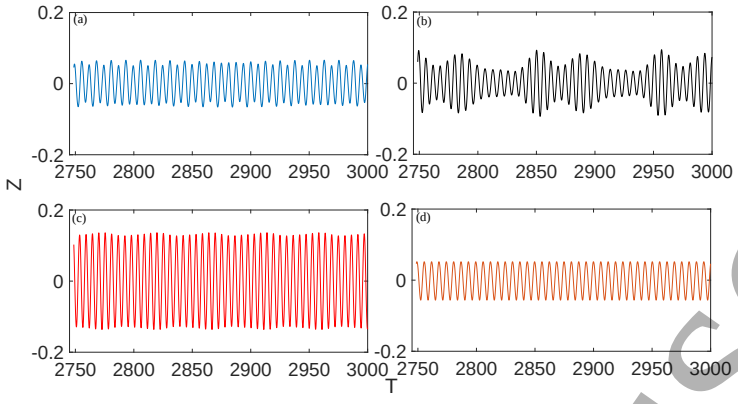

Figure 6. The calculation of time series versus time when parametric driving frequency $w_p = 1.52\omega_0$ in (a), $w_p = 1.88\omega_0$ in (b), $w_p = 2.27\omega_0$ in (c), and $w_p = 3\omega_0$ in (d).

amplitudes are gradually increased from 0.1× 1.24 μW to 60× 1.24 μW, 1 and 60 are two boundary values of the ratio range. By recording the peak values of the resonator, the bifurcation of amplitude versus ratio is given. It is shown in Fig. 7 (a) that the amplitudes exhibit a rich dynamical phenomenon that include period-doubling transition, period-chaos transition, chaos-period transition, etc. Though the bifurcation diagram of MEMS/NEMS resonators are not rarely seen in other reports[4][5], the bifurcation induced by laser through the form of cavity-less parametric driving is, to our best of knowledge, firstly reported. The results have the significance in terms of controlling and utilization of various dynamical states in NEMS resonator by touchless means. Similar result is also present in Fig. 7 (b), where the frequency of parametric driving is fixed at $w_p = 2.75\omega_0$. One can see the bifurcation phenomenon is again appeared. Detailed description is omitted here.

With the aim to know how the dynamics of the NEMS resonator behaves under the changing of three parameters, i.e., w_p, P_{ex0} and ω_d, a more detailed amplitude investigation is implemented. The results are given, respectively, in Fig. 8. It is seen in Fig. 8 (a) the amplitudes of the resonator are obliviously larger at $\omega_d = 1$ (see the right side of Fig. 8 (a)), and as the driving amplitude increases there are local brighter regions appearing due to the co-working mechanism between driving strength P_{ex0} and ω_d. From the left side of the Fig. 8 (a), the brighter region concentrated at $w_p \approx 2\omega_0$. This is actually consisted with Fig. 5, at which moment the parametric driving plays an amplifying effect. One also can see from the left side of Fig. 8 (a) that as the driving strength goes up the amplitude is getting larger, particularly when $w_p \approx 2\omega_0$. The largest amplitude of resonator is peaked at the intersection between surface $w_p = 2.1\omega_0$ and surface $\omega_d = 1.09\omega 0$. To provide a clearer picture, three slices taken from Fig. 8 (a) are presented in Fig. 8 (b). One can see that all the considered parameters w_p, ω_d and P_{ex0} play an important role in modulating the dynamics of the resonator. Specifically, the ω_d decides the occurrence of resonance. The w_p is directly related to the

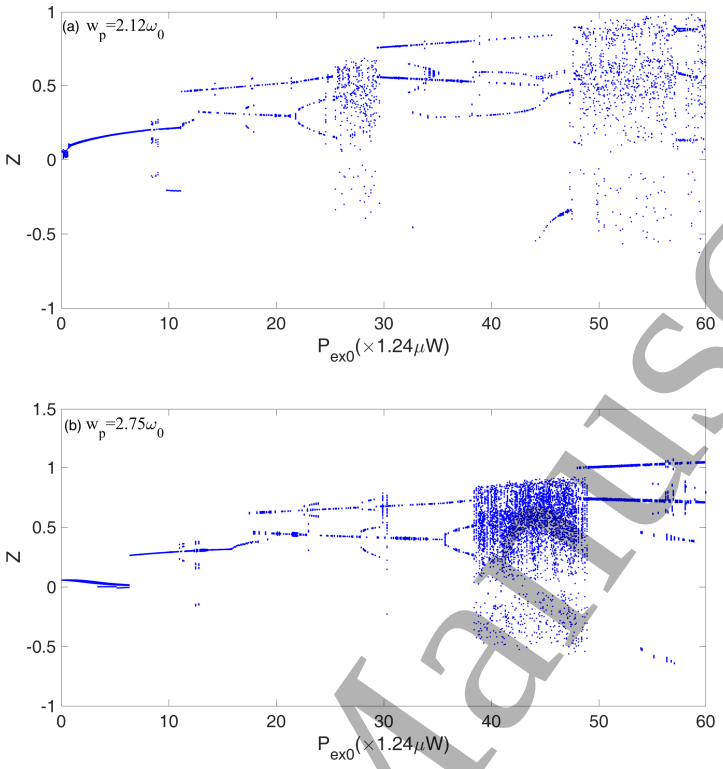

Figure 7. (a) Bifurcation diagram of GaAs resonator with parametric driving amplitude P_{ex0} varied in the range 0.1× 1.24 μW to 60× 1.24 μW and the driving frequency $w_p = 2.12\omega_0$. (b) Bifurcation diagram of GaAs resonator with parametric driving amplitude P_{ex0} varied in the range 0.1× 1.24 μW to 60× 1.24 μW and the driving frequency $w_p = 2.75\omega_0$.

amplification effect brought by laser parametric driving. The driving strength in terms of P_{ex0} can enhance the parametric driving effect. In Fig. 8 (b), the slice of $\omega_d = 1.09\omega_0$ confirms the statement, in which a "tongue" shape appears when w_p varies around $2\omega_0$.

3.3. Chaos Control

In this section, we consider the case when the NEMS resonator oscillates in chaotic state as shown in Fig. 9 (a), which can be reached by increasing the driving voltage V_{dc} and v_{ac} to 25 V. When the parametric driving $P_{ex} = P_{ex0}sin(w_p t)$ is applied with the amplitude of laser power P_{ex0} fixed as low as 24.8 nW, the chaotic state can be converted into periodic state, as shown in Fig. 9 (b-d), where parametric driving frequency are set as $w_p = 0.9\omega_0$, $w_p = 3.8\omega_0$ and $w_p = 4.4\omega_0$. It is shown that the chaotic time series are modulated into periodical shapes. The Max lyapunov Exponent (MLE) is always used for characterizing the dynamical state in nonlinear systems[27]. It is chaotic when MLE is positive, and vice versa. To confirm the results in Fig. 9, the MLE is calculated with w_p varying in the range of [0.5 10]ω_0 as shown in Fig. 10.

It is revealed that at a few points, including the special points selected by Fig. 9, the MLE of our considered nonlinear system is plunged into negative values, proving

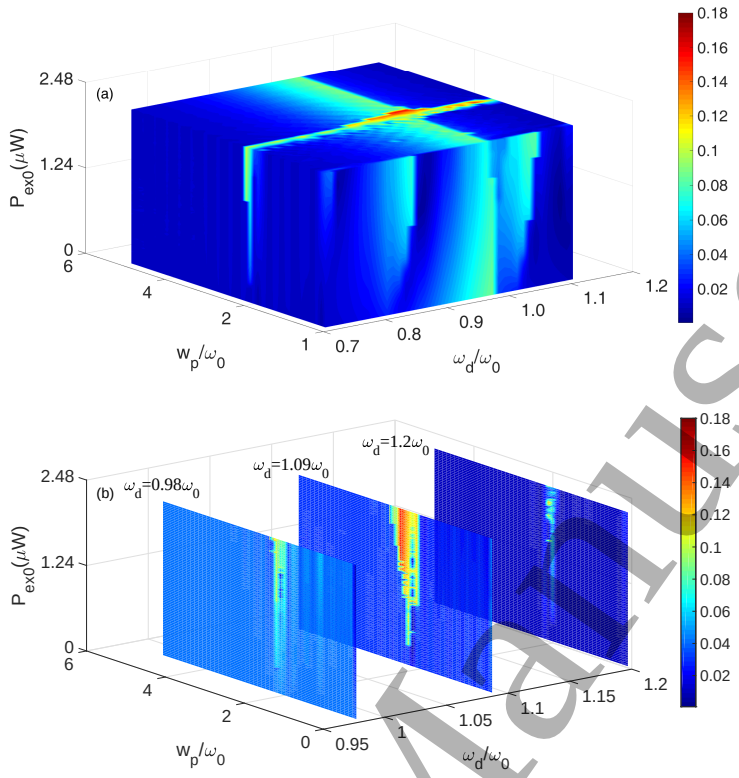

Figure 8. (a) The amplitude of GaAs resonator changes with parameters w_p, ω_d and P_{ex0} varied. (b) Three slices corresponding to $\omega_d = 0.98\omega_0$, $\omega_d = 1.09\omega_0$ and $\omega_d = 1.2\omega_0$ are taken from Fig. 8 (a).

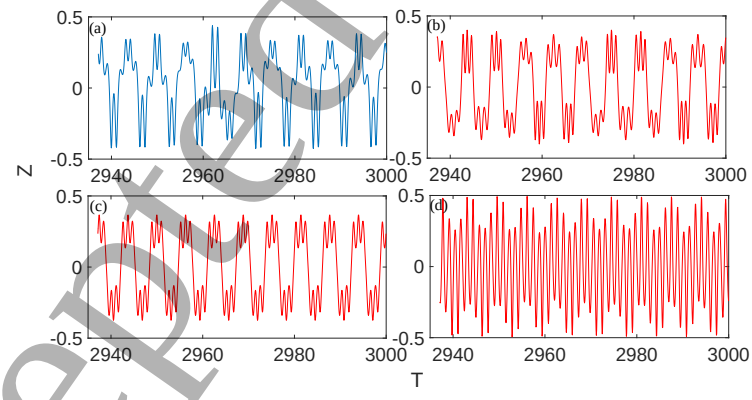

Figure 9. The chaotic state in (a), and parametric control using parametric laser driving with $w_p = 0.9\omega_0$ in (b), $w_p = 3.8\omega_0$ in (c) and $w_p = 4.4\omega_0$ in (d).

the chaos control effect attributed to parametric driving.

4. Conclusion

The nonlinear model for describing the dynamics of cavity-less opto-nanomechanical dynamical coupling process is constructed for the first time, which lays the foundation for

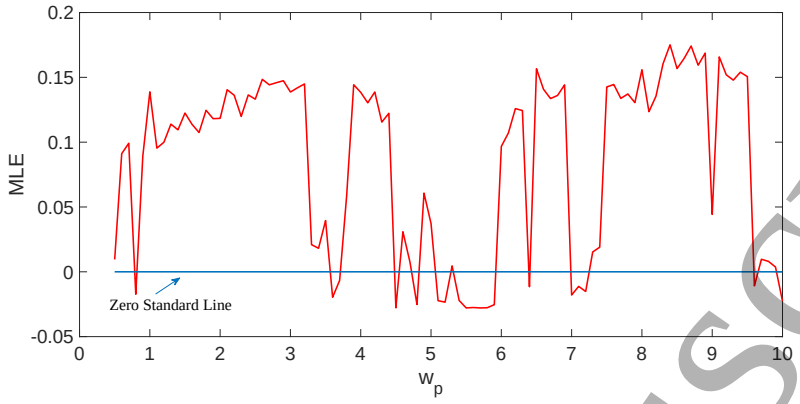

Figure 10. Max lyapunov Exponents (MLE) calculated with parametric laser driving frequency varying in the range of $[0.5\ 10]\omega_0$. The blue line is zero standard line.

further investigating unknown physics, particularly the nonlinear dynamics, behind the optomechanical systems/devices developed with cavity-less opto-mechanical coupling mechanism. Detailed numerical simulation shows that the laser injection can make an appealing effect in controlling and modulating the tiny NEMS resonators. Apart from the softening and hardening effect brought by laser, richer NEMS resonator dynamic response including variety of bifurcations can be achieved through applying laser parametric driving. Compared with conventional means such as capacitive and piezoelectric ways for changing the spring constant of resonator, the results revealed here prove that cavity-less laser manipulation works in a broader dynamical range extending into chaotic state, etc. The work sheds the light in developing novel NOEMS, and can also be employed for reading out with ultra-sensitively and manipulating the NEMS resonators.

References

[1] Jian Zhou; Nicolaie Moldovan; Liliana Stan; Haogang Cai; David A; Czaplewski; and Daniel Lpez, "Approaching the Strain-Free Limit in Ultrathin Nanomechanical Resonators", *Nano Lett*, 2020, 20, 8, pp. 5693C5698.

[2] Ghatge, M; Walters, G; Nishida, T; Tabrizian, R, "A 30-nm thick integrated hafnium zirconium oxide nano-electro-mechanical membrane resonator", *APPLIED PHYSICS LETTERS*, 2020, 116, 4, 043501.

[3] Vahid Qaradaghi; A. Ramezany; S. Babu; J. B. Lee; S. Pourkamali, "Nanoelectromechanical Disk Resonators as Highly Sensitive Mass Sensors", *IEEE Electron Device Letters*, 2018, 39, 11, 1744-1747.

[4] Gusso, A; Viana, RL; Mathias, AC; Caldas, IL, "Nonlinear dynamics and chaos in micro/nanoelectromechanical beam resonators actuated by two-sided electrodes", *CHAOS SOLITONS and FRACTALS*, 2019, 122, 6-16.

[5] Amorim, TD; Dantas, WG; Gusso, A, "Analysis of the chaotic regime of MEMS/NEMS fixed-fixed beam resonators using an improved 1DOF mode", *NONLINEAR DYNAMICS*, 2015, 79, 2, 967-981.

[6] Leonardo Midolo, Albert Schliesser and Andrea Fiore, "Nano-opto-electro-mechanical systems", *Nature Nanotechnology*, 2018, 13, 11-18.

[7] Shkarin, A. B. and Flowers-Jacobs, N. E. and Hoch, S. W. and Kashkanova, A. D. and Deutsch, C. and Reichel, J. and Harris, J. G. E., "Optically Mediated Hybridization between Two Mechanical Modes", *Physical Review Letters*, 2014, 112, 013602.

[8] Palomaki, TA, Teufel, JD, Simmonds, RW, Lehnert, K. W., "Entangling Mechanical Motion with Microwave Fields", *Science*, 2013, 342, 710-713.

[9] Zarko Zobenica, Rob W. van der Heijden, Maurangelo Petruzzella, Francesco Pagliano, Rick Leijssen, Tian Xia, Leonardo Midolo, Michele Cotrufo, YongJin Cho, Frank W.M. van Otten, Ewold Verhagen, Andrea Fiore, "Integrated nano-opto-electro-mechanical sensor for spectrometry and nanometrology", *Nature Communications*, 2017, 8. 2216, 1-8.

[10] Yuzhi Shi, Sha Xiong, Lip Ket Chin, Jingbo Zhang, Wee Ser, Jiuhui Wu, Tianning Chen, Zhenchuan Yang, Yilong Hao, Bo Liedberg, Peng Huat Yap, Din Ping Tsai, Cheng-Wei Qiu and Ai Qun Liu, "Nanometer-precision linear sorting with synchronized optofluidic dual barriers", *Science Advances*, 2018, 4, eaao0773.

[11] R. B. Karabalin, S. C. Masmanidis, and M. L. Roukes, "Efficient parametric amplification in high and very high frequency piezoelectric nanoelectromechanical systems", *Appl. Phys. Lett*, 2010, 97, 183101.

[12] Dustin W. Carr, Stephane Evoy, Lidija Sekaric, H. G. Craighead, and J. M. Parpia, "Parametric amplification in a torsional microresonator", *Appl. Phys. Lett*, 2000, 77, 1545.

[13] Ivan Favero and Florian Marquardt, "Focus on optomechanics", *New J. Phys*, 2014, 16, 085006.

[14] Bargatin, I. et al., "Large-scale integration of nanoelectromechanical systems for gas sensing applications", *Nano Lett.* 2012, 12, 1269-1274.

[15] Habraken, S. J. M., Stannigel, K., Lukin, M. D., Zoller, P and Rabl, P. "Continuous mode cooling and phonon routers for phononic quantum networks", *New J. Phys*, 2012, 14, 115004

[16] Hajime Okamoto, Takayuki Watanabe, Ryuichi Ohta, Koji Onomitsu, Hideki Gotoh, Tetsuomi Sogawa and Hiroshi Yamaguchi, "Cavity-less on-chip optomechanics using excitonic transitions in semiconductor heterostructures", *Nature Communications*, 2015, 6, 8478.

[17] Yuksel, M; Orhan, E; Yanik, C; Ari, AB; Demir, A; Hanay, MS, "Nonlinear Nanomechanical Mass Spectrometry at the Single-Nanoparticle Level", *Nano Letters*, 2019, 19, 6, 3583-3589.

[18] He, Ji Dong; Sun, Jia Sheng; Jiang, Jin Wu, "Nanomechanical resonators based on group IV element monolayers", *Nanotechnology* 2018, 29, 16, 165503

[19] Kang, Dong Keun; Yang, Hyun Ik; Kim, Chang Wan, "Thermal effects on mass detection sensitivity of carbon nanotube resonators in nonlinear oscillation regime", *Phyisca E-Low-Dimentional Systems and Nanostructures*, 2015, 74, 39-44.

[20] Nourmohammadi, Zahra; Mukherjee, Sankha; Joshi, Surabhi, "Methods for Atomistic Simulations of Linear and Nonlinear Damping in Nanomechanical Resonators", *Journal of Microelectromechanical Systems*, 2015, 24, 5, 1462-1470.

[21] Simsek, Mesut, "Nonlinear free vibration of a functionally graded nanobeam using nonlocal strain gradient theory and a novel Hamiltonian approach", *International Journal of Engineering Science*, 2016, 105, 12-17.

[22] E. Ciancio, R. C. Iotti and F. Rossi, "Gauge-invariant formulation of Fermi's golden rule: Application to high-field transport in semiconductors", *Europhysics Letters*, 2004, 65, 2

[23] Hajime Okamoto, Daisuke Ito, Koji Onomitsu, Haruki Sanada, Hideki Gotoh, Tetsuomi Sogawa and Hiroshi Yamaguchi, "Vibration Amplification, Damping, and Self-Oscillations in Micromechanical Resonators Induced by Optomechanical Coupling through Carrier Excitation", *Physical Review Letter*, 2011, 106, 036801.

[24] C. Herring and E. Vogt, "Transport and Deformation-Potential Theory for Many-Valley Semiconductors with Anisotropic Scattering", *Physical Review*, 1956, 101, 3, 944-961.

[25] R. B. Karabalin, S. C. Masmanidis, and M. L. Roukes, "Efficient parametric amplification in high and very high frequency piezoelectric nanoelectromechanical systems", *Applied Physics Letters*,

2010, 97, 183101

[26] D. Rugar and P. Griitter, "Mechanical Parametric Amplification and Thermomechanical Noise Squeezing", *Physical Review Letter*, 1991, 67, 6

[27] Jin, Leisheng; Guo, Yufeng; Ji, Xincun; Lijie Li, "Reconfigurable chaos in electro-optomechanical system with negative Duffing resonators", *Scitentific Reports*, 2017, 7, 4822.

Acknowledgments

The authors acknowledge the support from China Postdoctoral Science Foundation (No. 2019T120447).